Original Research

Shear type and magnitude affect aortic valve endothelial cell morphology, orientation, and differentiation

Nandini Deb[1], Mir S Ali[2], Ashley Mathews[1], Ya-Wen Chang[1] and Carla MR Lacerda[1]

[1]Department of Chemical Engineering, Texas Tech University, Lubbock, TX 79409-3121, USA; [2]Lewis Katz School of Medicine, Temple University, Philadelphia, PA 19140, USA

Corresponding author: Carla MR Lacerda. Email: carla.lacerda@ttu.edu

Impact statement

This work is important in heart valve pathophysiology as it describes details of valve endothelial cell morphology and mesenchymal protein expression along with actin microfilament orientation under physiologic and extreme shear stress condition. In this study, we used a parallel-plate device and evaluated morphological behavior of hundreds of cells in culture. Along with morphological parameters, analysis of actin order parameter and immunofluorescence experiments to detect VEC differentiation, we found that shear levels/duration affect VEC. The main changes in behaviors are loss of classic endothelial cuboidal morphology and gain of elongated shape, mesenchymal markers, and general alignment perpendicular to flow. Collectively, these findings improve our understanding of valve endothelial cell differentiation so that engineered living heart valves can be developed to support patients with heart valve diseases.

Abstract

Valvular endothelial cells line the outer layer of heart valves and can withstand shear forces caused by blood flow. In contrast to vascular endothelial cells, there is limited amount of research over valvular endothelial cells. For this reason, the exact physiologic behavior of valvular endothelial cells is unclear. Prior studies have concluded that valvular endothelial cells align perpendicularly to the direction of blood flow, while vascular endothelial cells align parallel to blood flow. Other studies have suggested that different ranges of shear stress uniquely impact the behavior of valvular endothelial cells. The goal of this study was to characterize the response of valvular endothelial cell under different types, magnitudes, and durations of shear stress. In this work, the results demonstrated that with increased shear rate and duration of exposure, valvular endothelial cells no longer possessed the traditional cuboidal morphology. Instead through the change in cell circularity and aspect ratio, valvular endothelial cells aligned in an organized manner. In addition, different forms of shear exposure caused the area and circularity of valvular endothelial cells to decrease while inducing mesenchymal transformation validated through αSMA and TGFβ_1 expression. This is the first investigation showing that valvular endothelial cells alignment is not as straightforward as once thought (perpendicular to flow). Different types and magnitudes of shear induce different local behaviors. This is also the first demonstration of valvular endothelial cells undergoing EndMT without chemical inducers on a soft surface *in vitro*. Findings from this study provide insights to understanding the pathophysiology of valvular endothelial cells which can potentially propel future artificial engineered heart valves.

Keywords: Aortic valve, endothelial cells, shear stress, endothelial to mesenchymal transformation, morphology, protein expression

***Experimental Biology and Medicine* 2021; 246: 2278–2289. DOI: 10.1177/15353702211023359**

Introduction

Heart valves are complex tri-layered cardiac structures that maintain unidirectional blood flow by opening and closing.[1] Each heart valve consists of valve leaflets also known as valve cusps. During every cardiac cycle, valve leaflets face shear stress due to blood flow. Among the four valves, the aortic valve (AV) allows blood to flow to the aorta from the left ventricle with a very high transvalvular pressure of 80 mmHg.[2] The outermost layer of valve cusps is a monolayer of valvular endothelial cells (VECs), enveloping interstitial cells (VICs) embedded into the inner extra cellular matrix (ECM).[3] Two sides of the AV, ventricular side and aortic side experience two distinct patterns of blood flow. The ventricular side experiences a high laminar shear stress, while the aortic side experiences a low oscillatory shear stress.[4] A study by Yap *et al.* measured the *in vivo* shear stress magnitude utilizing a two-component laser Doppler velocimetry on the aortic valve leaflet. They reported that under physiologic conditions, the shear stress

on the ventricular side was 70 dyne/cm^2, whereas it was 23 dyne/cm^2 on the aortic side.[5,6] These mechanical stimuli directly impact tissue hemostasis and structural integrity.

VECs experience shear stress due to high pressure blood flow and the dynamic motion of valve leaflets. It has been established by others that high shear enables porcine VECs to align in perpendicular direction to the flow.[7–9] However, this behavior contrasts with the nature of human VECs. Holliday *et al.*[10] showed that human VECs from aortic valve align in the direction of the fluid flow. This difference in orientation of VECs in porcine and human aortic valve suggests different shear stresses may result in different trends in cell alignment and morphologies. In addition, VECs from both of these species revealed significant differences in their protein expression on the aortic and the ventricular side.[10,11] Previous studies have demonstrated that shear stresses induce different responses in VECs morphology, expression of markers such as αSMA, F-actin, PECAM-1, when cells were confined in a very small region facing the fluid shear.[8,9,12] Shear stress modulates stress fibers to reorient, allowing VECs to change their morphology. While the high shear-facing ventricular side adapts to the complex hemodynamic environment due to unidirectional blood flow, the low oscillatory shear aortic side is more prone to cardiovascular diseases such as calcification and lesion formation because of differences in transcriptional profiles.[13] Therefore, it can be concluded that fluid shear stress maintains the valve physiology and abnormal levels may contribute to pathological transformation of the heart valve.

To withstand high shear stress, valve tissues require continuous matrix remodeling. Endothelial mesenchymal transformation (EndMT) is the process through which VECs remodel the embedding tissue, in both embryonic and adult valves.[14,15] The role of EndMT in the adult valve is as of yet controversial.[14–18] Inflammatory cytokines (i.e. TGF-β, TNF-α) and mechanical stresses (shear stress, cyclic strain) are found to be responsible for inducing EndMT in the adult heart valve.[12,14,16,19] During the EndMT process, VECs lose cell–cell contacts and acquire mesenchymal markers as they invade the inner ECM.[20] To better understand valvular EndMT, it is crucial to determine a role for endothelial cell transformation in valvular pathophysiology.

The aim of this study is to evaluate the effect of different types, durations, and magnitudes of shear stresses on cell alignment, quantitative morphological parameters, and EndMT markers. We employed a modified parallel plate platform to study primary porcine VECs to describe VEC scalar order parameter, a variable that describes actin fiber orientation. This is the first study to link shear type and magnitude, to VEC orientation, determined quantitively by the scalar order parameter, to endothelial to mesenchymal transformation on a soft substrate.

Materials and methods

Cell isolation and culture

Fresh porcine hearts were collected from the local abattoir (All Hale Meats, Wolfforth, TX) and transported into the lab on ice. Aortic leaflets were dissected and washed once with phosphate-buffered saline (PBS) (1× PBS, 137 mM sodium chloride, 4.3 mM sodium phosphate dibasic, 2.7 mM potassium chloride, and 1.46 mM potassium phosphate monobasic) that contained 2% amphotericin b/penicillin/streptomycin (Quality Biological, Gaithersburg, MD, USA). Once the leaflets were properly washed, they were incubated with 1200 U/mL collagenase solution (Sigma-Aldrich, St. Louis, MO, USA) for 15 min at 37°C under a humidified atmosphere with 5% CO_2. This collagenase solution was prepared into fresh medium containing Dulbecco's modified eagle medium (DMEM, Dulbecco's modified Eagle medium, Corning Life Sciences, Tewksbury, MA, USA), along with 10% fetal bovine serum (FBS) (Atlanta Biologicals, Flowery Branch, GA, USA) and 1% amphotericin b/penicillin/streptomycin. After 15 min of incubation, the valve leaflets were taken out of the collagenase solution leaving suspended VECs in the solution. The collagenase solution concentrated with VECs was then centrifuged for 5 min at 1100 r/min. After the centrifugation, VECs were settled down as a pellet at the bottom of the vial. The VEC pellet was resuspended into the heparin medium (50 U/mL heparin (Sigma-Aldrich, St. Louis, MO, USA) in DMEM, 10% FBS, and 1% amphotericin b/penicillin/streptomycin, filter-sterilized). The VECs were then seeded onto 6-well plates at a density of 2.4×10^4 cells/cm^2. The cells were maintained on the culture plate until 80% confluence and the medium was changed every two days. When the cells reached 80% confluency, they were detached using 0.125% trypsin solution (Sigma-Aldrich, St. Louis, MO, USA) and utilized for the experiments. For all types of experiments, only passages three to five were used.

Substrate preparation

Liquid polydimethylsiloxane (PDMS, Sylgard, Dow corning) was prepared and baked at 57°C overnight using 20:1 base to curing agent ratio. Regular PDMS (made according to 10:1 base to curing agent) is too stiff to provide VEC cultures a comparable physiologic *in vivo* environment. Here a softer PDMS (20:1 base vs. curing agent ratio) was used to act as a supporting matrix, enabling growth (without dedifferentiation), and resistive of shear and folding. In details, 2 g Sylgard 184 silicone elastomer base was mixed with 0.1 g Sylgard 184 silicone elastomer curing agent resulting in a soft PDMS gel. On the following day, the surface of the PDMS gel was treated with 0.25 mM sulfo-succinimidyl 6–(4′-azido-2′-nitrophenylamino) hexanoate crosslinker (Fisher Scientific) and placed under an ultraviolet light for 30 min (302 nm wavelength, 1.9 mW/cm^2 irradiance). Following the UV treatment, 200 μg/mL type I bovine collagen (Advanced Biomatrix, San Diego, CA) in PBS-1X was applied on the surface and left for 4 h at 37°C with 5% CO2. After 4 h incubation, the surface of the PDMS gel was washed with PBS-1X. The VECs were seeded on the treated PDMS at a density of 2.4×10^4 cells/cm^2.

Device loading

After seeding cells onto the PDMS gel, the cells were allowed to grow overnight. The next day, a modified parallel plate

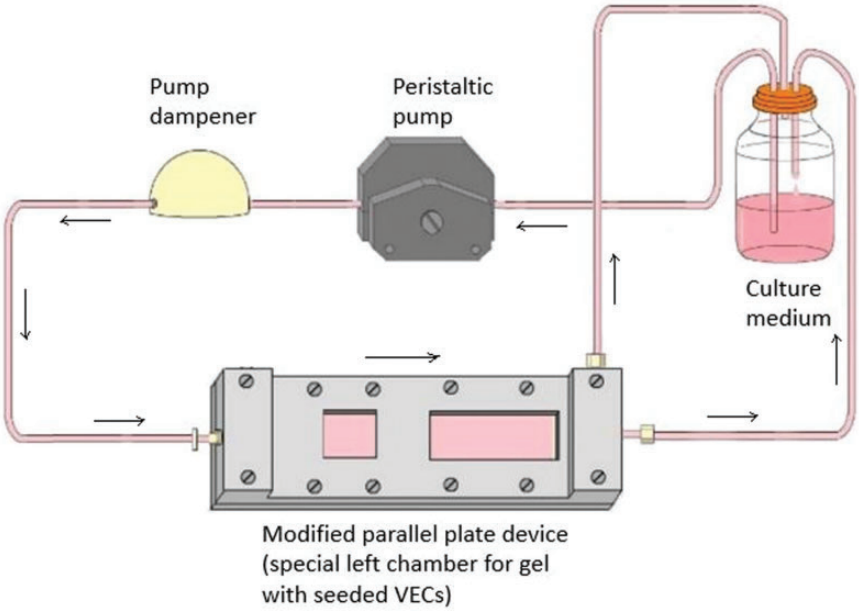

Figure 1. Experimental set up[21] for fluid shear on VECs seeded on soft PDMS. The left rectangular chamber contains cells seeded PDMS gel. Pulse dampener was used for introducing laminar flow. Black arrowheads indicate direction of fluid flow. (A color version of this figure is available in the online journal.)

device (Figure 1) was set up. This device was redesigned using the established parallel plate device.[21] In this modified flow device, there was a separate chamber with larger height for allowing spacing of polymer gel or hydrogel seeded with cells. The PDMS gel that contained a monolayer of VECs was placed on the left chamber of the device. Fresh heparin medium was used as fluid and a peristaltic pump was used for maintaining volumetric flow rate of the medium. All the equipment utilized, including the plates and piping, were sterilized prior to use. For laminar shear flow, a pulse dampener was placed in between peristaltic pump and the inlet of the parallel plate device. VECs were stimulated with laminar and pulsatile volumetric flow through the parallel plate device. The shear stress (τ) generated from volumetric flow (Q) was calculated using the equation: $\tau = 6Q\mu/h^2w$,[22–24] where μ is the viscosity of the medium, h is the height of the chamber from the PDMS gel floor, and w is the width of the chamber. Three different flow rates were applied on the VECs to introduce shear stresses of $-0\,\text{dyne/cm}^2$ (static), $20\,\text{dyne/cm}^2$, $35\,\text{dyne/cm}^2$. For this study, to mimic the physiologic *in vivo* condition, $20\,\text{dyne/cm}^2$ shear stress was applied. The maximum empirical limit for VECs until which cells can withstand induced shear stress for 48 h was $35\,\text{dyne/cm}^2$. Beyond that limit, cells tended to wash away from the culture. Therefore, $35\,\text{dyne/cm}^2$ was considered a pathologic condition.[25,26] The effect of these three different flow rates was observed for a duration of 24 h and 48 h. The application of shear stress on cells was maintained at 37°C under a humidified atmosphere with 5% CO_2 within an incubator.

Immunofluorescence staining

After applying fluid shear, the monolayer VECs on PDMS gels were fixed with 3.7% paraformaldehyde (Thermo Fisher Scientific, Waltham, MA, USA) for 40 min. Then the gel was washed with MES buffer (10 mM 2-(N-morpholino) ethanesulfonic acid, 10 mM sodium chloride, 1.5 mM magnesium chloride, 10% glycerol, 100 KIU aprotinin, pH = 6.2) three times and 0.1% Igepal (Sigma-Aldrich, St. Louis, MO, USA) in MES was used to enable cell permeability for 10 min; 1% goat serum (MP Biomedicals, Santa Ana, CA, USA) in MES was applied for 40 min for blocking non-specific binding. Following goat serum application, αSMA was tagged with mouse monoclonal primary antibody (Thermo Scientific, Waltham, MA, USA) for 1.5 h. This step was followed by tagging with DyLight 488 conjugated goat anti-mouse IgG secondary antibody (Thermo Scientific, Waltham, MA, USA) for another 1.5 h. Then TGFβ_1 was tagged by rabbit monoclonal primary antibody (Thermo Scientific, Waltham, MA, USA) for 1.5 h with DyLight 594 conjugated goat anti-rabbit IgG secondary antibody (Thermo Scientific, Waltham, MA, USA) following next 1.5 h. After the protein staining, actin microfilaments were tagged with rhodamine-phalloidin (Cytoskeleton, Denver, CO, USA) for 40 min and DAPI (4′,6-diamidino-2-phenylindole, Molecular Probes, Eugene, OR, USA) was applied for 10 min for nuclei staining. Three times MES wash is involved in between each step. Leica widefield microscopy system equipped with Leica Application Suite X imaging software (AF6000, Leica Microsystems, Wetzlar, Germany) was used for acquiring fluorescence images. Briefly, the culture substrate was placed on a glass coverslip and fixed on the microscope stage; 20×/0.50 NA DRY objective was used for microscopic evaluation. Excitation/emission filter cube with a non-laser light source (LED) was utilized for illuminating the sample. Light source intensity and camera were maintained at 100%. Camera configuration was set at 8 bits with 40 MHz gamma mode and 1 gamma value. As the cells were tagged with fluorescent antibodies, images were captured as grey scale image under four

specific excitation wavelengths of 405, 488, 568, and 594 nm, and were artificially colored as blue, green, orange, and far red, respectively. During image acquisition, exposure time was held constant across samples and experimental groups for given fluorescence filters. Image resolution and pixel information were also acquired for analyses.

Data analysis

Morphological parameters of cells were detected as described previously using ImageJ software (Image processing and analysis in Java by NIH Image, National Institute of Health, Bethesda, MD).[27,28] Data were generated to quantify cell area, circularity, and aspect ratio of individual cells. Cell circularity is defined by the equation $4\pi A/P^2$, where A is the cell area and P is the cell perimeter. Cell circularity close to one represents a perfect circle, while a circularity of zero represents a straight line. On the other hand, cell aspect ratio is defined by the ratio of major axis length to minor axis length. The MATLAB image processing toolbox was used to evaluate protein expression and orientation tensor. αSMA and TGFβ_1 protein expressions were evaluated for all groups. Fluorescence images were first segmented into green and red channels. These single channel images were then converted into a greyscale image. From the greyscale images, backgrounds were subtracted from a region of interest and mean normalized intensities were evaluated.

Based on the differences in size and length of actin fibers and nuclei (cylindrical vs. circular), the effect of shear would appear more prominently on thin long cytoskeleton fibers compared to rounded nuclei. Here, actin filaments have been analyzed to evaluate the effect of shear stress on stress fiber orientation. Actin orientation tensor heat map was generated using the MATLAB image processing toolbox followed by implementing a method developed by Ellis *et al.*[29] This procedure enabled to visualize the change in actin orientation and quantify degree of order, defined as order parameter S (equation (1))

$$S = \frac{1}{2} < 3\ cos^2\theta_m - 1 > \qquad (1)$$

where θ_m represents orientation angle between the vertical axis and the cell long axes.[30] The value of S ranged from zero to one. S equals zero signifies completely random orientation and heat maps show a variety of colors, whereas S equals one represents the highest level of order and organization and as a consequence, heat map colors become more uniform. Mathematically, $S = 1$, when most actin fibers are aligned with the main axis, θ_m approaches zero. When $S = 0$, actin fibers show no alignment with any preferential direction, and $<cos^2\theta> \sim 1/3$.

All quantitative results were presented here as mean (SD). A minimum of 200 cells from three images for each biological replicate were analyzed for every experimental group. All experiments were performed for at least three biological replicates. Kruskal–Wallis ANOVA on ranks and multiple comparison tests were performed to determine statistically significance differences among groups. *P*-values less than 0.05 was considered as significant.

Results

Shear stress rate and magnitude induce morphological change

Regardless of culture duration (Figure 2), VECs maintained their cell area ($P > 0.05$) when no fluid shear (0 dyne/cm^2) was present. As the shear rate increased, VECs exhibited a decrease in the cell area and circularity, while increasing the aspect ratio. At 0 dyne/cm^2, the cell area was 547.37 (41.50) μm^2. In comparison to static culture ($P < 0.0001$), the cell area for both 20 dyne/cm^2 and 35 dyne/cm^2 decreased in shear types, intensities, and durations. For the durations of 24 h and 48 h, when placed under laminar flow, the cell area decreased with 20 dyne/cm^2 and 35 dyne/cm^2 shear stress. There were no significant differences ($P > 0.05$) between the same magnitude shear groups. At 24 h and 48 h, similar effects were expressed by 20 dyne/cm^2 and 35 dyne/cm^2. Similarly, pulsatile flow amongst the same shear stress groups exhibited no notable changes during 24 h and 48 h. These findings show that the duration of shear flow, for both laminar and pulsatile flow conditions, does not influence the cell area to change. This suggests that cell area mostly depends upon the magnitude of shear flow.

As the cell area decreased with increasing shear stress, cell circularity also decreased (Figure 3). For laminar flow, at both 24 h and 48 h, cell circularity decreased with increasing fluid shear. From the experiment, circularity for 24 h, the shear flow ($P > 0.05$) was similar in both 20 dyne/cm^2 and 35 dyne/cm^2. However, for shear stress condition at 48 h, this was not the case as there was a significant difference ($P < 0.0001$) seen. Contrarily, for pulsatile flow condition, circularity decreases drastically at 48 h 35 dyne/cm^2 shear stress compared to 24 h 35 dyne/cm^2 shear stress ($P < 0.0001$), though there are no significant differences ($P > 0.05$) of cell circularity under 20 dyne/cm^2 pulsatile shear stress at 24 hand 48 h. For both laminar flow and pulsatile flow, change in cell aspect ratio is similar ($P > 0.05$) under 20 dyne/cm^2 shear stress regardless of the duration of shear (Figure 4). Alternatively, cell aspect ratio did not change much ($P > 0.05$) at 35 dyne/cm^2 shear stress for 24 h and 48 h. However, at pulsatile flow compared to 24 h, there was a notable effect on increase of cell aspect ratio at 35 dyne/cm^2 shear stress at 48 h.

Circularity correlates strongly with aspect ratio

Cell area and circularity hold a weak correlation towards one another (Figure 5). The dependence of cell area and circularity is unlikely and there is minimal correlation ($r^2 = 0.01$) under different magnitudes of shear stress. Conversely, the correlation between aspect ratio and circularity showed an inverse dependence (Figure 6). Cell circularity and aspect ratio are negatively correlated with each other. As the circularity decreases, cell aspect ratio increases with increasing fluid shear. Compared to 24 h, 48-h shear stress induced a strong correlation ($r^2 = 0.6$ vs. $r^2 = 0.7$) for both laminar and pulsatile flow.

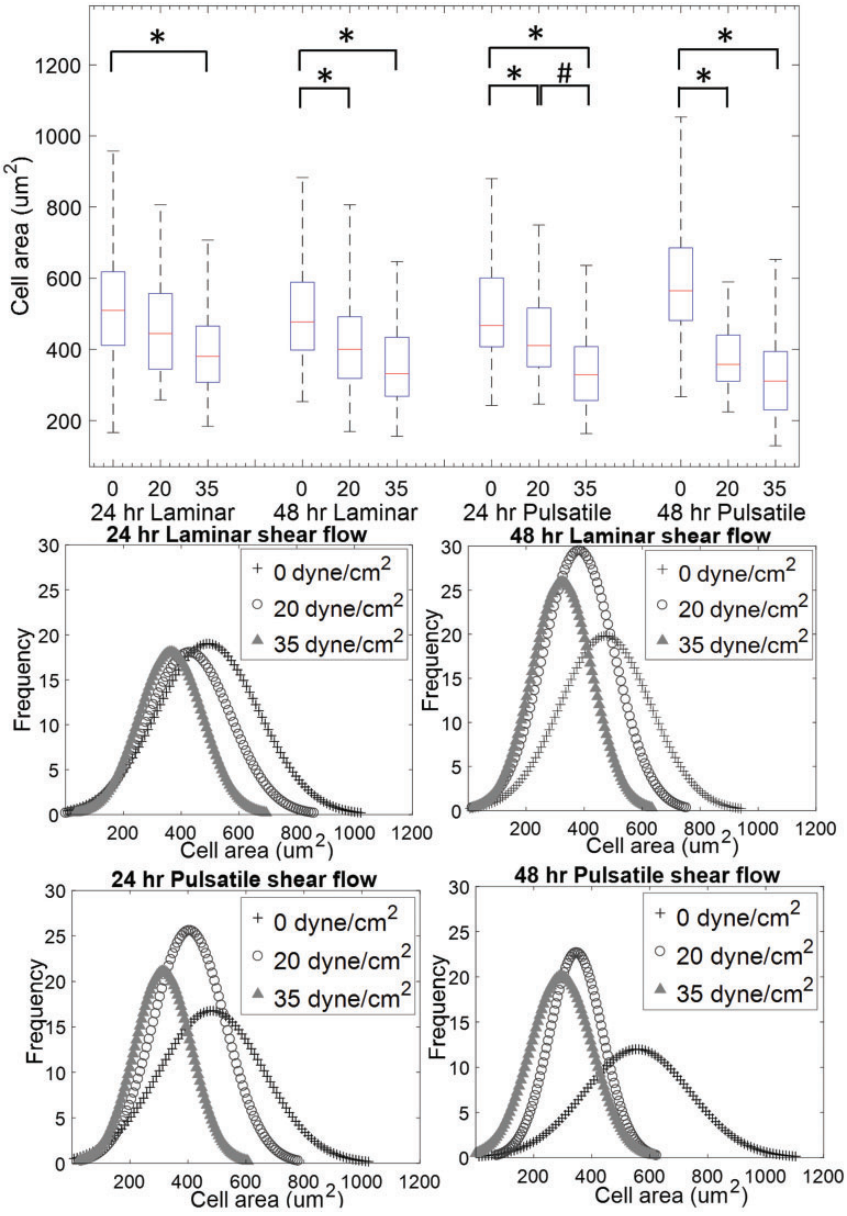

Figure 2. Box plots and distribution curves of cell areas for laminar and pulsatile shear experiments. As shear stress magnitudes increase, cell areas decrease. n= 203–237, $^*P < 0.05$ between 0 dyne/cm^2 and 20 dyne/cm^2 or 35 dyne/cm^2 groups. $^{\#}P < 0.05$ between 20 dyne/cm^2 and 35 dyne/cm^2. (A color version of this figure is available in the online journal.)

VEC reorganize with the increase of shear magnitude and duration

In addition to cortical actin, VECs started to show stress fibers with application of shear stress (Figure 7 laminar flow, Figure 8 pulsatile flow) compared to static condition. Accompanied with increased fluid shear and duration, VECs became more aligned. To better visualize the orientation of actin fibers, a heat map was used. Less color diversity represented higher cell alignment, whereas more color diversity and patterns represented disorganization. As the shear stress magnitude increased, the heat map showed a more uniform color distribution. In all static groups (0 dyne/cm^2), the heat map contains a diverse range of color, meaning random distribution. As shear stress increased, the heat map deviates from more diverse to more uniform green-blue distribution. This means that the actin fibers were aligned in a more uniform manner. Scalar order parameter, S, states how organized actin fibers are in a scale of 0 to 1. All shear groups had a higher S values compared to static control groups (Figure 9). That implies that shear-exposed groups had more aligned actin fibers than the static control groups. Compared to laminar shear group, pulsatile shear groups had actin fibers that were more aligned as well. These findings showed that the alignment of actin fibers correlated also with the nature of shear flow.

Shear stress induces differentiation in VECs

VEC transformation was shown through αSMA (Figure 10) and TGFβ_1 expression (Figure 11). In VECs, αSMA

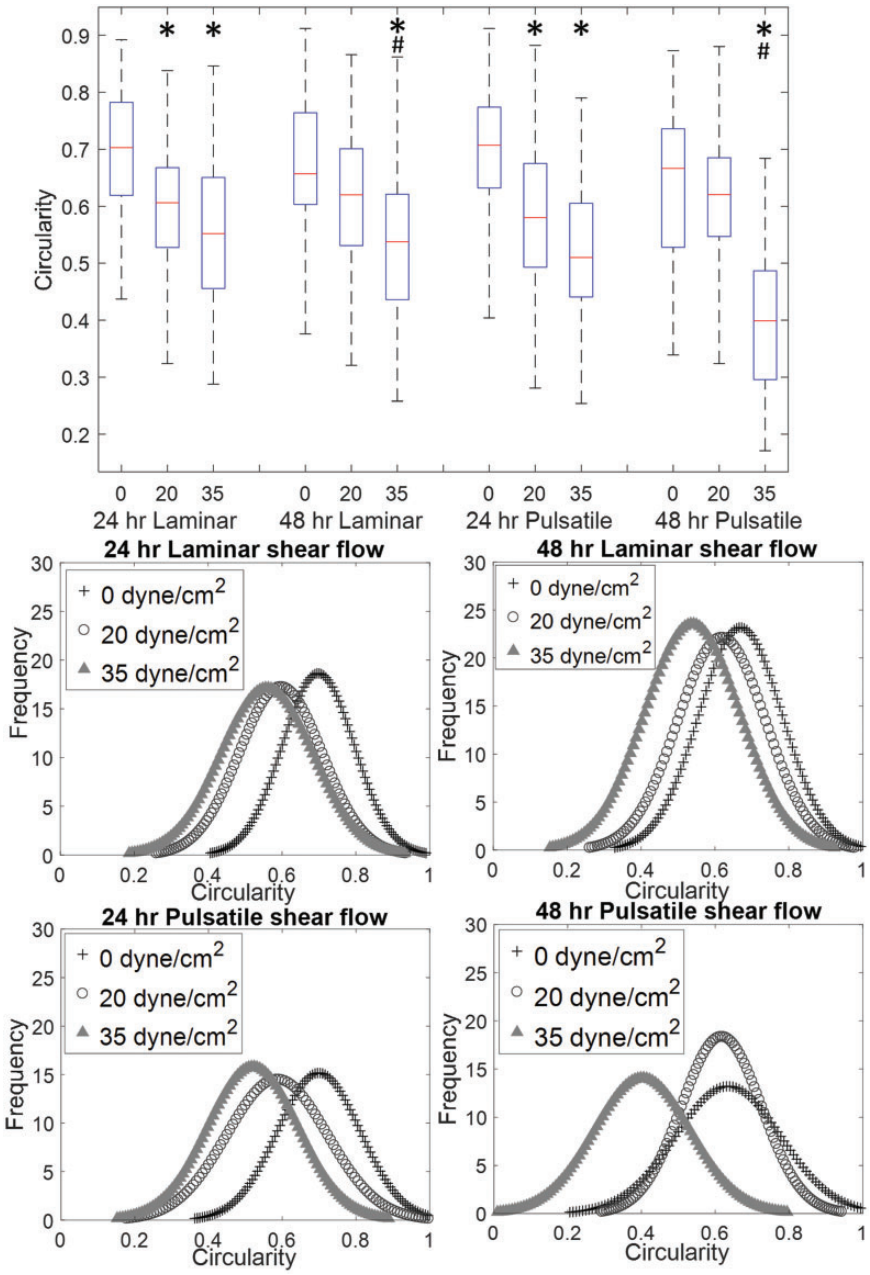

Figure 3. Box plots and distribution curves of cell circularity for laminar and pulsatile shear experiments. As shear stress magnitudes increase, cell circularities decrease. $n = 203–237$, $^{*}P < 0.05$ between 0 dyne/cm^2 and 20 dyne/cm^2 or 35 dyne/cm^2 groups. $^{\#}P < 0.05$ between 20 dyne/cm^2 and 35 dyne/cm^2. (A color version of this figure is available in the online journal.)

expression increased from 2 a.u. (arbitrary units) to 55 a.u. with increasing shear magnitude. Pulsatile flow induced stronger αSMA expression than laminar flow. At 0 dyne/cm^2, the αSMA staining for both 24 h and 48 h laminar and pulsatile flow conditions were very faint. As shear stress increased, cells showed enhanced αSMA expression. As a result, as the pixel brightness increased with rising shear magnitude, resulted into higher mean intensity. In laminar flow conditions, αSMA expression increased gradually with increasing shear, where expression was significantly higher in pathologic flow condition (intensity 26–29 a.u.) compared to physiologic flow (intensity 14–19 a.u.) ($P < 0.05$). While in pulsatile flow, there was not any significant difference in αSMA expression between physiologic and pathologic condition. Following the same trend as αSMA, TGFβ_1 expression also increased with increasing shear stress up to 56 a.u. with negligible amount of expression in 0 dyne/cm^2 flow condition (intensity ~0–1 a.u.) (Figure 11). However, the TGFβ_1 expression was stronger in pulsatile flow pathologic condition (intensity 48–56 a.u.) compared to physiologic condition (intensity 25–29 a.u.) ($P < 0.05$). There was not much difference between expression levels in laminar flow physiologic and pathologic condition (intensity 20–26 a.u.). Expression levels of both αSMA and TGFβ_1 suggest that VECs acquire a mesenchymal/myofibroblastic phenotype as they face any physiologic or pathologic shear flow. Along with the change in

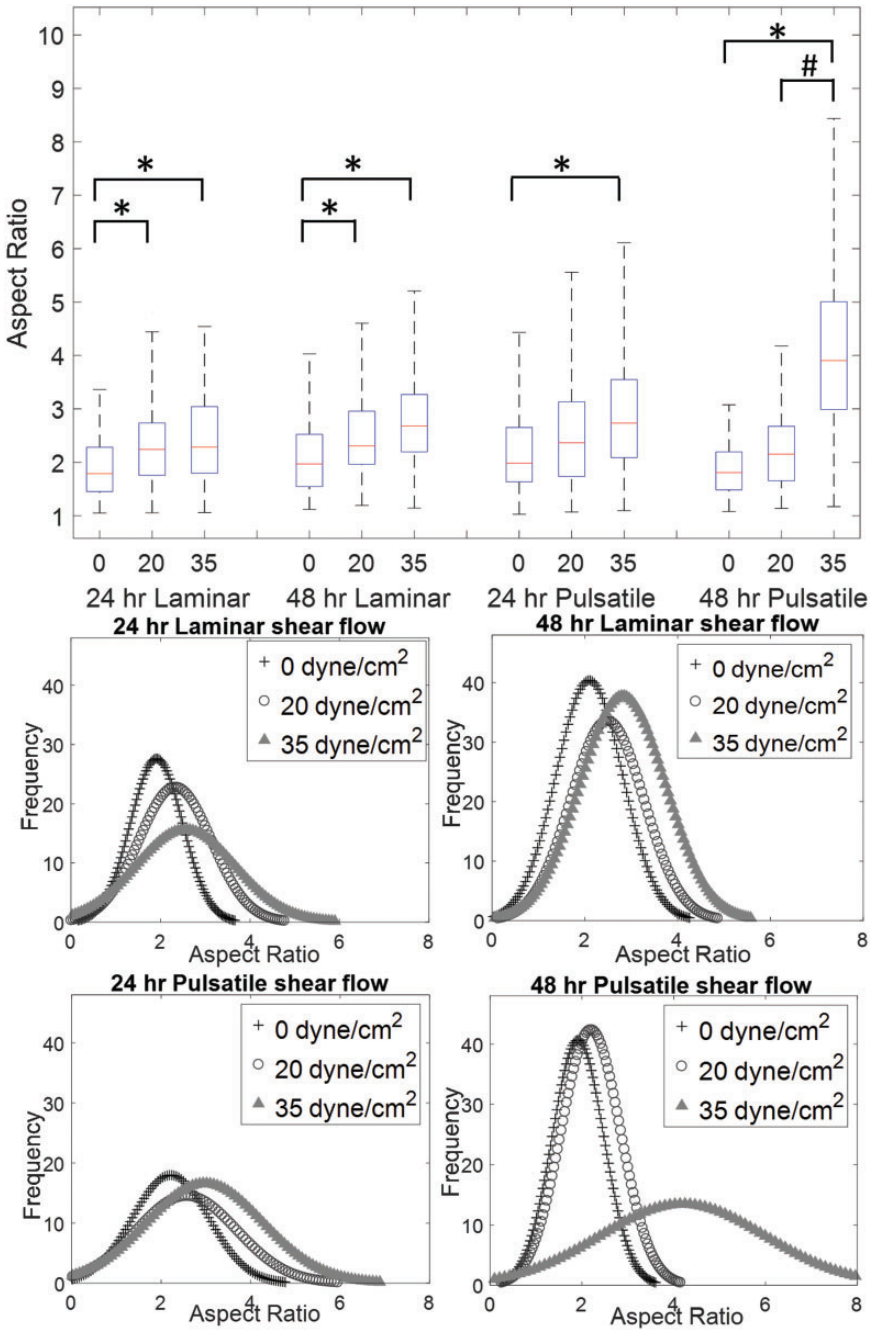

Figure 4. Box plots and distribution curves of cell aspect ratios for laminar and pulsatile shear experiments. As shear stress magnitudes increase, cell aspect ratios increase. $n = 203–237$, $^{*}P < 0.05$ between 0 dyne/cm^2 and 20 dyne/cm^2 or 35 dyne/cm^2 groups. $^{\#}P < 0.05$ between 20 dyne/cm^2 and 35 dyne/cm^2. (A color version of this figure is available in the online journal.)

morphology and actin fiber reorganization, these results suggest that EndMT is induced by fluid shear on VECs.

Discussion

The ECM of aortic valve cusps consists of collagen, proteoglycan, and elastin.[31] These components provide variable mechanical properties and structural integrity for the tissue. The interplay between the mechanical environment and biochemical signals holds responsibility for tissue hemostasis and degeneration.[32] To mimic an exact *in vivo* biomechanical environment, cells should be cultured on soft substrates instead of plastic or glass coverslips. To date, most VEC studies have focused primarily on microchannels to induce shear flow on VECs.[8,9,12] For our study, a modified parallel plate design was introduced to allow cells to grow on a soft substrate, while maintaining their innate quiescence. To avoid the possibility of high fluid shear folding or washing the gel, a soft PDMS was utilized during the shear stress application (measured Young's modulus 0.495 (0.02) MPa, the same order of magnitude of the stiffness of an aortic valve leaflet[33]). Given that VECs can withstand approximately 70 dyne/cm^2 peak shear stress on the ventricular side, the extreme shear stress experienced by the

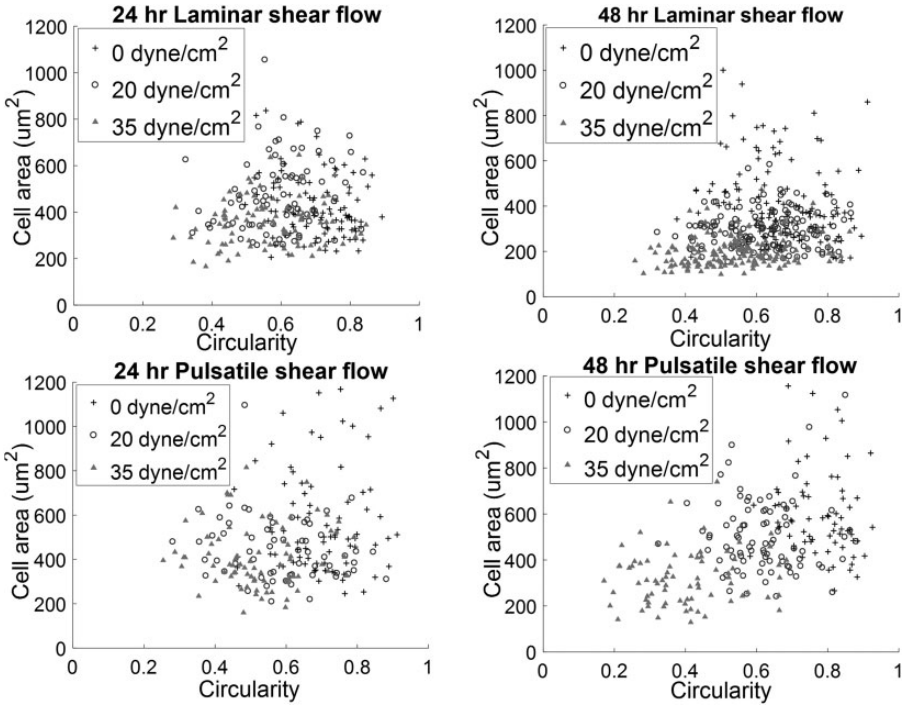

Figure 5. Correlation plots showing the low correlation between circularity and cell area. For any given circularity, increased shear stress magnitude decreases cell area.

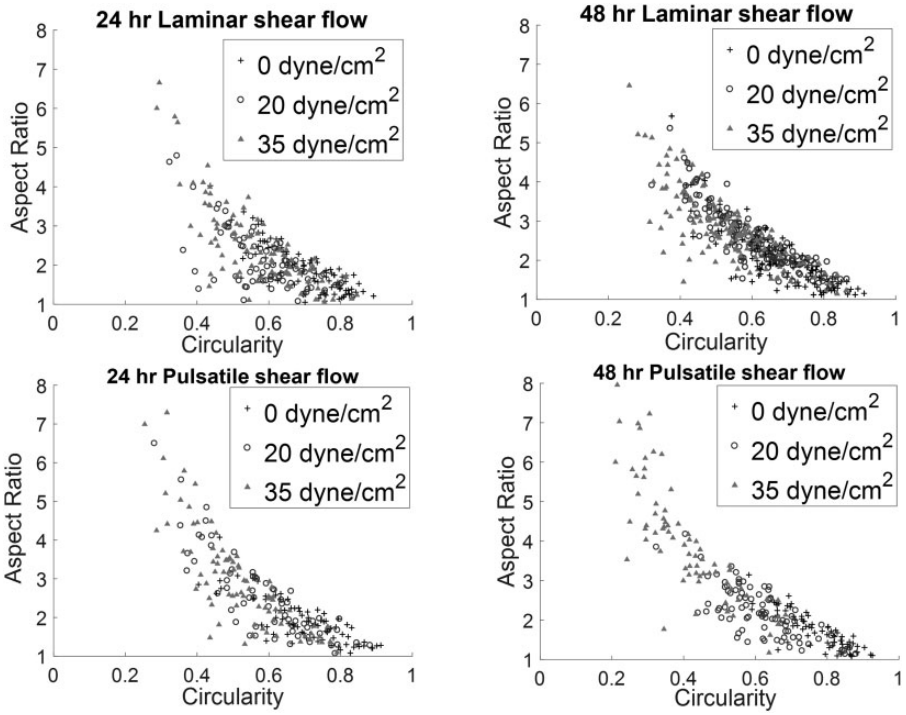

Figure 6. Correlation plots showing inverse dependence of aspect ratio on circularity.

valve only for short bursts of time,[5] 20 dyne/cm^2 is considered the average shear stress across the valve during each cardiac cycle.[34] However, this matrix does not enable the migration of cells through the substrate due to shear stress.

Scanning electron micrographs of aortic valves show that VECs align circumferentially on the valve leaflets which is in perpendicular to the direction of blood flow.[7] Previous *in vitro* studies have also reported the orientation of VECs under different fluid shear conditions.[8,9,12,35] Steady laminar shear stress (20 dyne/cm^2) enables VEC actin fibers to align in a perpendicular direction to the flow along the elongated cell shape.[8,12,35] Young *et al.*

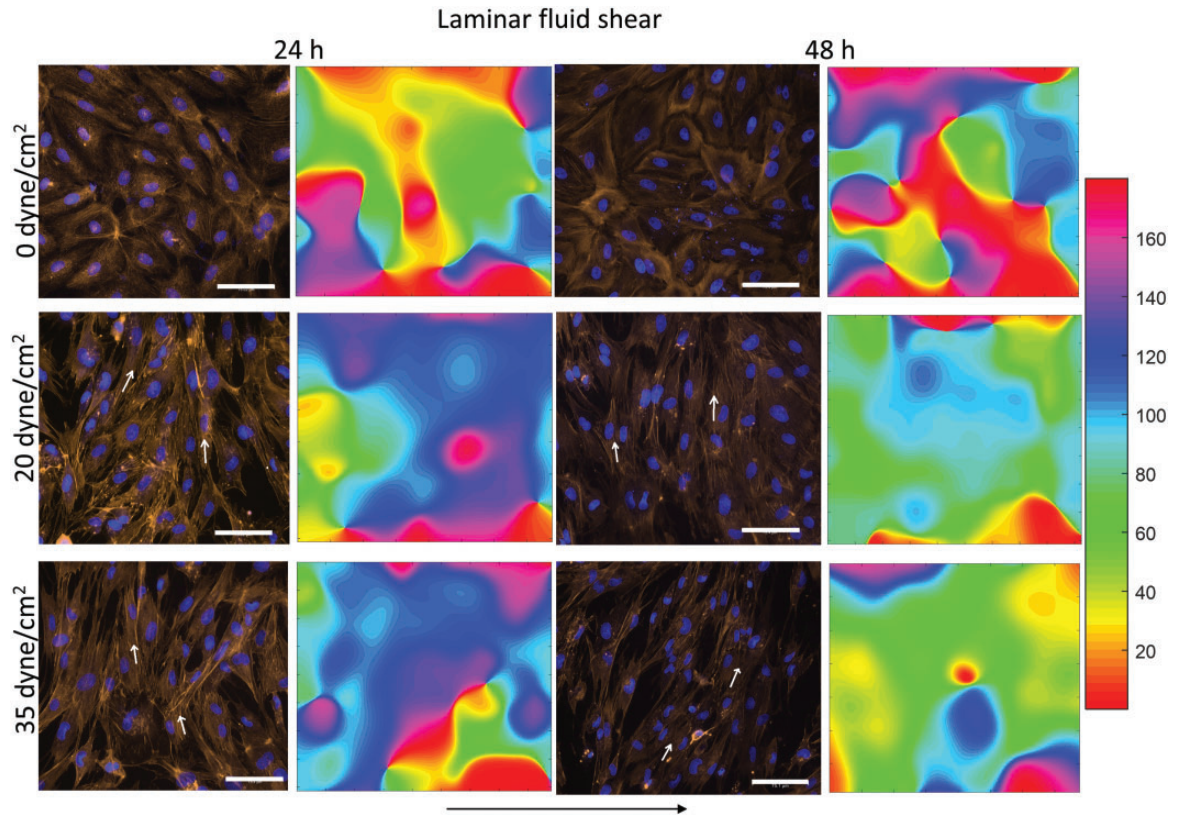

Figure 7. Micrographs and heat maps for experiments with laminar shear. Micrographs include DAPI nuclear stain (blue) and rhodamine-phalloidin stain of F-actin (orange). Scale bars represent 75 μm. Micrographs and heat maps indicate that increased shear stress magnitudes increase cell organization—cell alignment on micrographs and less color variation on heat maps. Black arrowhead represents the fluid flow direction, white arrowhead represents alignment direction of actin fibers.

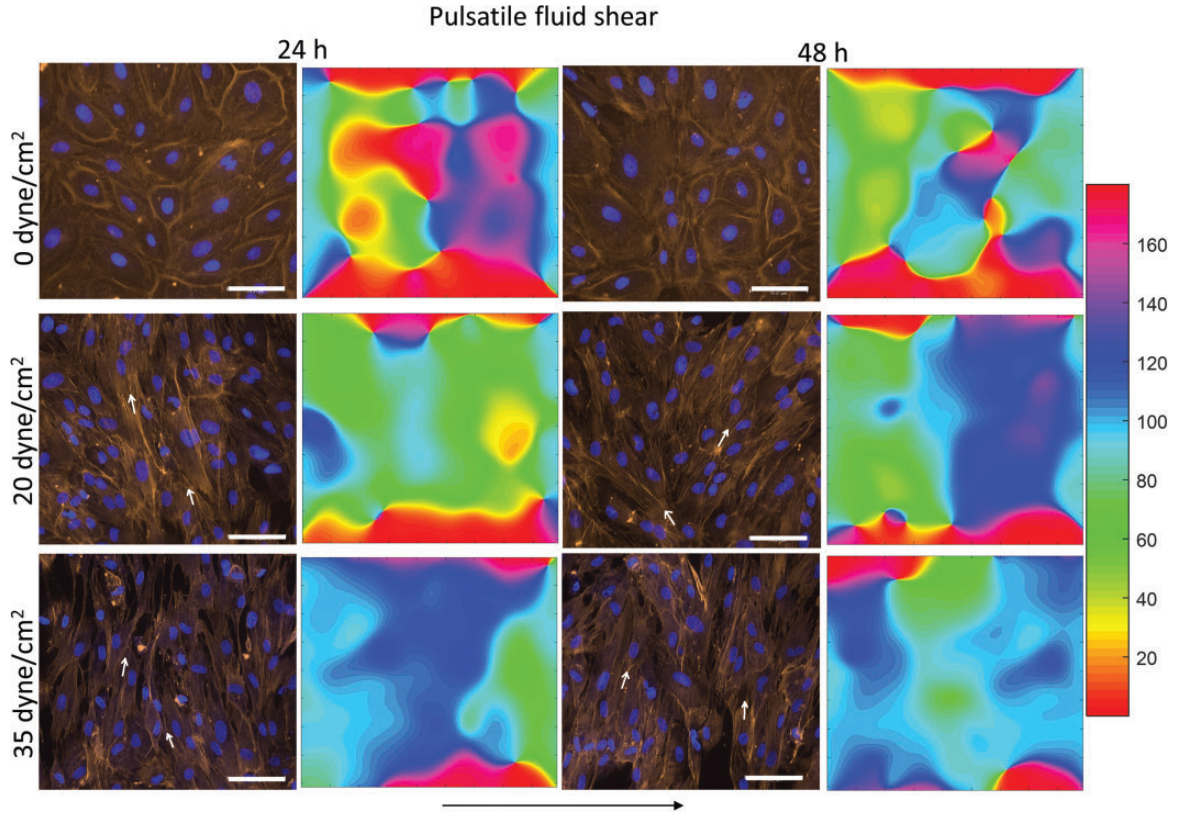

Figure 8. Micrographs and heat maps for experiments with pulsatile shear. Micrographs include DAPI nuclear stain (blue) and rhodamine-phalloidin stain of F-actin (orange). Scale bars represent 75 μm. Micrographs and heat maps indicate that increased shear stress magnitudes increase cell organization—cell alignment on micrographs and less color variation on heat maps. Black arrowhead represents the fluid flow direction, white arrowhead represents alignment direction of actin fibers.

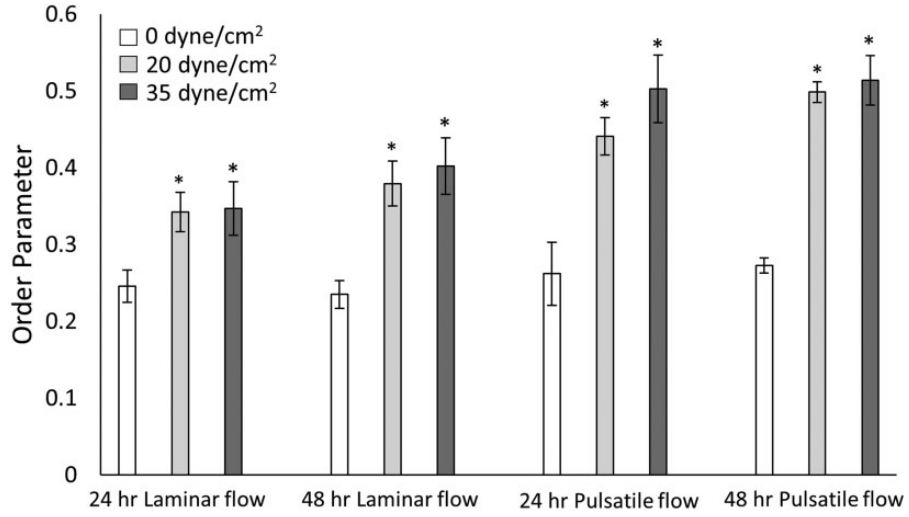

Figure 9. Actin fiber scalar order parameters (with SD) for all the shear groups, $^{*}P < 0.05$ between 0 dyne/cm^2 and 20 dyne/cm^2 or 35 dyne/cm^2 groups.

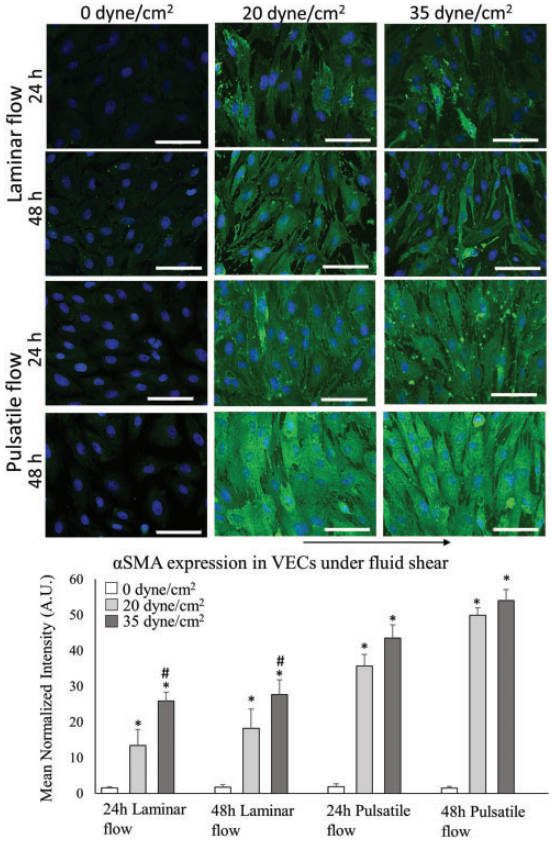

Figure 10. Micrographs and distribution plots of expression levels of αSMA. Micrographs include DAPI nuclear stain (blue) and αSMA (green). Scale bars represent 100 μm. Black arrowhead represents the fluid flow direction. Bar chart represents the intensity levels of αSMA increase with increasing shear stress magnitude, a potential indicator of cellular activation. $n = 217$–242, $^{*}P < 0.05$ between 0 dyne/cm^2 and 20 dyne/cm^2 or 35 dyne/cm^2 groups. $^{\#}P < 0.05$ between 20 dyne/cm^2 and 35 dyne/cm^2. (A color version of this figure is available in the online journal.)

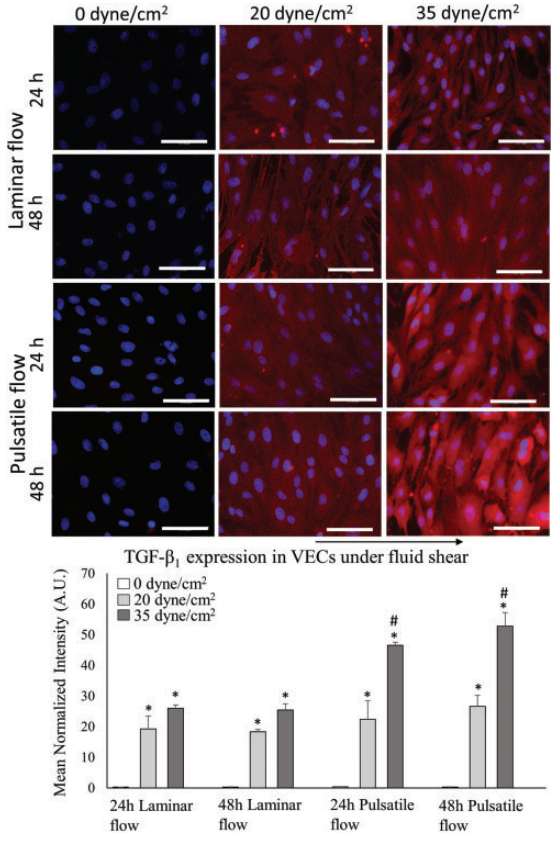

Figure 11. Micrographs and distribution plots of expression levels of TGFβ_1. Micrographs include DAPI nuclear stain (blue) and TGFβ_1 (red). Scale bars represent 100 μm. Black arrowhead represents the fluid flow direction. Bar chart represents the intensity levels of TGFβ_1 increase with increasing shear stress magnitude, a potential indicator of cellular activation. $n = 217$–242, $^{*}P < 0.05$ between 0 dyne/cm^2 and 20 dyne/cm^2 or 35 dyne/cm^2 groups. $^{\#}P < 0.05$ between 20 dyne/cm^2 and 35 dyne/cm^2. (A color version of this figure is available in the online journal.)

investigated high shear stress (110 dyne/cm^2, 220 dyne/cm^2) effects on VECs adhesion on underlying substrate in a microfluidic platform.[36] This study reported that VECs cannot withstand such high level of shear stress for 12 min without detachment. A recent study from Lee *et al.* reported a threshold limit for shear stress of 5 dyne/cm^2, below which VECs do not align *in vitro*.[9] However, both, stiff substrate and soft hydrogels enabled VECs to elongate

and align perpendicularly to flow direction under fluid shear stress *in vitro*.[9,12,37] There is a strong correlation between endothelial cell morphology and the mechanical environment.[8,12,38] Shear stress pattern is a major determinant at the early stage of the heart valve development in zebra fish.[39] Previous *in vitro* studies reported change in VECs morphology under 20 dyne/cm^2 laminar shear stress compared to static culture.[8,12] With the increase of the duration of the shear stress, VECs tend to have more aligned F-actin with reduced shape index and increased aspect ratio.[8,9]

Our results validated the similar findings from previous studies. Under both laminar and pulsatile flow, VECs cell area and circularity decreased when aspect ratio increased. However, the alignment and change in shape index of VECs vary with the pattern and magnitude of mechanical stress. Different levels and durations of stress induce different local response in VECs. As VECs face shear stress, actin fibers become more oriented and realign in a way that minimizes the effects of shear stress introduced on them.[40] This explains why under fluid shear VECs become aligned with more organized actin fibers (Figures 7 and 8). A previous study showed that, when VECs faced cyclic strain on anisotropic substrate, the orientational order parameter for actin fibers was high (0.8).[19] In this study, we reported scalar order parameter to quantify the probability of actin alignment under fluid shear stress. The order parameter value increases with increased shear stress magnitude and duration (Figure 9).

Furthermore, αSMA and TGFβ_1 were used as markers of EndMT. αSMA is an established mesenchymal marker that is incorporated with stress fibers and cell contractility.[41,42] Previous studies have reported that the types of shear stress have an effect on the expression level of αSMA.[9,12] Meanwhile, TGFβ_1 is known to be responsible for introducing EndMT in VECs.[16,43–45] Porcine, ovine, and human VECs and VICs incubated with TGFβ_1 showed enhanced expression of αSMA and stress fiber formation.[16,46,47] However, αSMA expression is less pronounced in VEC-VIC coculture in response to TGFβ_1 compared to VEC single culture.[48] VEC biological functions such as EndMT potential, tissue repair, and proliferation have been shown to decline, along with a decrease in αSMA expression, when VECs are supplemented with TGFβ_1.[49] Previously, altered shear stress was reported to enhance TGFβ_1 expression in aortic valve leaflet.[25,50] Our results confirmed that increased shear stress magnitude and duration collectively enhanced both αSMA (Figure 10) and TGFβ_1 (Figure 11) protein expression, while static cultures do not show the same trends. This strongly suggests that VECs undergo differentiation under shear stress without any chemical inducer and acquire a mesenchymal phenotype *in vitro*.

Conclusions

This is the first study to link shear type and magnitude, to VEC orientation, determined quantitively by the scalar order parameter, to endothelial to mesenchymal transformation on a soft substrate. Our study provides understanding on VECs behavior under different patterns and magnitudes of shear stress, mimicking physiologic and pathologic conditions. Results of this study support the effects of laminar and pulsatile flow conditions on VEC morphology, actin orientation, and differentiation. Specifically, our investigation showed that VEC alignment is not as straightforward as once thought (perpendicular to flow). Different types and magnitudes of shear induce different local behaviors. This is also the first demonstration of VECs undergoing EndMT without chemical inducers on a soft surface *in vitro*. Results obtained from this study can increase the current understanding of the complex heart valve hemodynamic environment, which plays an important role in heart valve diseases.

AUTHORS' CONTRIBUTIONS

ND, MSA, and CMRL participated in the design, experimentation, analysis, and interpretation of the studies; ND, YWC, and CMRL contributed to the analysis of the data; ND, AM, and CMRL conducted the review of the manuscript. CMRL provided conceptualization, project administration, financial support, and final approval.

ACKNOWLEDGMENTS

We thank All Hale Meats for providing us with porcine hearts.

DECLARATION OF CONFLICTING INTERESTS

The author(s) declared no potential conflicts of interest with respect to the research, authorship, and/or publication of this article.

FUNDING

The author(s) disclosed receipt of the following financial support for the research, authorship, and/or publication of this article: This study was supported by startup funds provided to Carla M. R. Lacerda by Texas Tech University.

ORCID iDs

Nandini Deb https://orcid.org/0000-0001-6568-0826
Carla MR Lacerda https://orcid.org/0000-0003-3571-0750

REFERENCES

1. Sacks MS, Yoganathan AP. Heart valve function: a biomechanical perspective. *Philos Trans R Soc Lond B Biol Sci* 2007;**362**:1369–91
2. Guyton AC. *Textbook of medical physiology*. Philadelphia: W. B. Saunders Company, 1976
3. Tao G, Kotick JD, Lincoln J. Heart valve development, maintenance, and disease: the role of endothelial cells. *Curr Top Dev Biol* 2012;**100**:203–32
4. Arjunon S, Rathan S, Jo H, Yoganathan AP. Aortic valve: mechanical environment and mechanobiology. *Ann Biomed Eng* 2013;**41**:1331–46
5. Yap CH, Saikrishnan N, Yoganathan AP. Experimental measurement of dynamic fluid shear stress on the ventricular surface of the aortic valve leaflet. *Biomech Model Mechanobiol* 2012;**11**:231–44
6. Yap CH, Saikrishnan N, Tamilselvan G, Yoganathan AP. Experimental measurement of dynamic fluid shear stress on the aortic surface of the aortic valve leaflet. *Biomech Model Mechanobiol* 2012;**11**:171–82
7. Deck JD. Endothelial cell orientation on aortic valve leaflets. *Cardiovasc Res* 1986;**20**:760–7

8. Butcher JT, Penrod AM, Garcia AJ, Nerem RM. Unique morphology and focal adhesion development of valvular endothelial cells in static and fluid flow environments. *Arterioscler Thromb Vasc Biol* 2004;**24**:1429–34
9. Lee J, Estlack Z, Somaweera H, Wang X, Lacerda CMR, Kim J. A microfluidic cardiac flow profile generator for studying the effect of shear stress on valvular endothelial cells. *Lab Chip* 2018;**18**:2946–54
10. Holliday CJ, Ankeny RF, Jo H, Nerem RM. Discovery of shear- and side-specific mRNAs and miRNAs in human aortic valvular endothelial cells. *Am J Physiol Heart Circ Physiol* 2011;**301**:H856–67
11. Simmons CA, Grant GR, Manduchi E, Davies PF. Spatial heterogeneity of endothelial phenotypes correlates with side-specific vulnerability to calcification in normal porcine aortic valves. *Circ Res* 2005;**96**:792–9
12. Mahler GJ, Frendl CM, Cao Q, Butcher JT. Effects of shear stress pattern and magnitude on mesenchymal transformation and invasion of aortic valve endothelial cells. *Biotechnol Bioeng* 2014;**111**:2326–37
13. Butcher JT, Simmons CA, Warnock JN. Mechanobiology of the aortic heart valve. *J Heart Valve Dis* 2008;**17**:62–73
14. Mahler GJ, Farrar EJ, Butcher JT. Inflammatory cytokines promote mesenchymal transformation in embryonic and adult valve endothelial cells. *Arterioscler Thromb Vasc Biol* 2013;**33**:121–30
15. Bischoff J. Endothelial-to-Mesenchymal transition purposeful versus maladaptive differentiation. *Circ Res* 2019;**124**:1163–5
16. Paranya G, Vineberg S, Dvorin E, Kaushal S, Roth SJ, Rabkin E, Schoen FJ, Bischoff J. Aortic valve endothelial cells undergo transforming growth factor-beta-mediated and non-transforming growth factor-beta-mediated transdifferentiation in vitro. *Am J Pathol* 2001;**159**:1335–43
17. Piera-Velazquez S, Jimenez SA. Molecular mechanisms of endothelial to mesenchymal cell transition (EndoMT) in experimentally induced fibrotic diseases. *Fibrogenesis Tissue Repair* 2012;**5**:S7
18. Rieder F, Kessler SP, West GA, Bhilocha S, de la Motte C, Sadler TM, Gopalan B, Stylianou E, Fiocchi C. Inflammation-induced endothelial-to-mesenchymal transition: a novel mechanism of intestinal fibrosis. *Am J Pathol* 2011;**179**:2660–73
19. Balachandran K, Alford PW, Wylie-Sears J, Goss JA, Grosberg A, Bischoff J, Aikawa E, Levine RA, Parker KK. Cyclic strain induces dual-mode endothelial-mesenchymal transformation of the cardiac valve. *Proc Natl Acad Sci U S A* 2011;**108**:19943–8
20. Nakajima Y, Mironov V, Yamagishi T, Nakamura H, Markwald RR. Expression of smooth muscle alpha-actin in mesenchymal cells during formation of avian endocardial cushion tissue: a role for transforming growth factor beta3. *Dev Dyn* 1997;**209**:296–309
21. Lane WO, Jantzen AE, Carlon TA, Jamiolkowski RM, Grenet JE, Ley MM, Haseltine JM, Galinat LJ, Lin FH, Allen JD, Truskey GA, Achneck HE. Parallel-plate flow chamber and continuous flow circuit to evaluate endothelial progenitor cells under laminar flow shear stress. *J Vis Exp* 2012;**59**:3349
22. Bhat VD, Truskey GA, Reichert WM. Fibronectin and avidin-biotin as a heterogeneous ligand system for enhanced endothelial cell adhesion. *J Biomed Mater Res* 1998;**41**:377–85
23. Wong AK, PLL, Boroda N, Rosenberg SR, Rabbany SY. A Parallel-Plate flow chamber for mechanical characterization of endothelial cells exposed to laminar shear stress. *Cell Mol Bioeng* 2016;**9**:127–38
24. Bird RB, Stewart WE, Lightfoot EN. *Transport phenomena*. New York: John Wiley and Sons, Inc., 1960.
25. Hoehn D, Sun L, Sucosky P. Role of pathologic shear stress alterations in aortic valve endothelial activation. *Cardiovasc Eng Tech* 2010;**1**:165–78
26. Esmerats JF, Heath J, Rezvan A, Jo H. Hemodynamics and mechanobiology of aortic valve calcification. *Biosyst Biorobot* 2016;**9**:237–61
27. Schneider CA, Rasband WS, Eliceiri KW. NIH image to ImageJ: 25 years of image analysis. *Nat Methods* 2012;**9**:671–5
28. Ali MS, Deb N, Wang X, Rahman M, Christopher GF, Lacerda CMR. Correlation between valvular interstitial cell morphology and phenotypes: a novel way to detect activation. *Tissue Cell* 2018;**54**:38–46
29. Ellis PW, Pearce DJG, Chang YWG, G, Giomi L, Fernandez-Nieves A. Curvature-induced defect unbinding and dynamics in active nematic toroids. *Nature Phys* 2018;**14**:85–90
30. Jones RAL. Soft condensed matter. *Oxford master series in condensed matter physics*. New York: Oxford University Press, 2002, p. 195
31. Hinton RB, Yutzey KE. Heart valve structure and function in development and disease. *Annu Rev Physiol* 2011;**73**:29–46
32. Wang H, Leinwand LA, Anseth KS. Cardiac valve cells and their microenvironment–insights from in vitro studies. *Nat Rev Cardiol* 2014;**11**:715–27
33. Missirlis YF, Chong M. Aortic valve mechanics–part I: material properties of natural porcine aortic valves. *J Bioeng* 1978;**2**:287–300
34. Weston MW, LaBorde DV, Yoganathan AP. Estimation of the shear stress on the surface of an aortic valve leaflet. *Ann Biomed Eng* 1999;**27**:572–9
35. Butcher JT, Tressel S, Johnson T, Turner D, Sorescu G, Jo H, Nerem RM. Transcriptional profiles of valvular and vascular endothelial cells reveal phenotypic differences: influence of shear stress. *Arterioscler Thromb Vasc Biol* 2006;**26**:69–77
36. Young EW, Wheeler AR, Simmons CA. Matrix-dependent adhesion of vascular and valvular endothelial cells in microfluidic channels. *Lab Chip* 2007;**7**:1759–66
37. Butcher JT, Nerem RM. Valvular endothelial cells regulate the phenotype of interstitial cells in co-culture: effects of steady shear stress. *Tissue Eng* 2006;**12**:905–15
38. Butcher JT, Nerem RM. Valvular endothelial cells and the mechanoregulation of valvular pathology. *Philos Trans R Soc Lond B Biol Sci* 2007;**362**:1445–57
39. Boselli F, Steed E, Freund JB, Vermot J. Anisotropic shear stress patterns predict the orientation of convergent tissue movements in the embryonic heart. *Development* 2017;**144**:4322–7
40. Barbee KA, Davies PF, Lal R. Shear stress-induced reorganization of the surface topography of living endothelial cells imaged by atomic force microscopy. *Circ Res* 1994;**74**:163–71
41. Farrar EJ, Butcher JT. Heterogeneous susceptibility of valve endothelial cells to mesenchymal transformation in response to TNFalpha. *Ann Biomed Eng* 2014;**42**:149–61
42. Armstrong EJ, Bischoff J. Heart valve development: endothelial cell signaling and differentiation. *Circ Res* 2004;**95**:459–70
43. Huk DJ, Austin BF, Horne TE, Hinton RB, Ray WC, Heistad DD, Lincoln J. Valve endothelial Cell-Derived Tgfbeta1 signaling promotes nuclear localization of Sox9 in interstitial cells associated with attenuated calcification. *Arterioscler Thromb Vasc Biol* 2016;**36**:328–38
44. Zhong A, Mirzaei Z, Simmons CA. The roles of matrix stiffness and ss-Catenin signaling in endothelial-to-Mesenchymal transition of aortic valve endothelial cells. *Cardiovasc Eng Technol* 2018;**9**:158–67
45. Dvorin EL, Wylie-Sears J, Kaushal S, Martin DP, Bischoff J. Quantitative evaluation of endothelial progenitors and cardiac valve endothelial cells: proliferation and differentiation on poly-glycolic acid/poly-4-hydroxybutyrate scaffold in response to vascular endothelial growth factor and transforming growth factor beta1. *Tissue Eng* 2003;**9**:487–93
46. Wang X, Ali MS, Lacerda CMR. A Three-Dimensional Collagen-Elastin scaffold for heart valve tissue engineering. *Bioengineering* 2018;**5**:69
47. Walker GA, Masters KS, Shah DN, Anseth KS, Leinwand LA. Valvular myofibroblast activation by transforming growth factor-beta: implications for pathological extracellular matrix remodeling in heart valve disease. *Circ Res* 2004;**95**:253–60
48. Hjortnaes J, Shapero K, Goettsch C, Hutcheson JD, Keegan J, Kluin J, Mayer JE, Bischoff J, Aikawa E. Valvular interstitial cells suppress calcification of valvular endothelial cells. *Atherosclerosis* 2015;**242**:251–60
49. Anstine LJ, Bobba C, Ghadiali S, Lincoln J. Growth and maturation of heart valves leads to changes in endothelial cell distribution, impaired function, decreased metabolism and reduced cell proliferation. *J Mol Cell Cardiol* 2016;**100**:72–82
50. Sucosky P, Balachandran K, Elhammali A, Jo H, Yoganathan AP. Altered shear stress stimulates upregulation of endothelial VCAM-1 and ICAM-1 in a BMP-4- and TGF-beta1-dependent pathway. *Arterioscler Thromb Vasc Biol* 2009;**29**:254–60

(Received December 2, 2020, Accepted May 19, 2021)